NANOMATERIALS

A customizable class of colloidal-quantum-dot spasers and plasmonic amplifiers

Stephan J. P. Kress,[1]* Jian Cui,[1]* Patrik Rohner,[2] David K. Kim,[1] Felipe V. Antolinez,[1] Karl-Augustin Zaininger,[1] Sriharsha V. Jayanti,[1] Patrizia Richner,[2] Kevin M. McPeak,[1] Dimos Poulikakos,[2] David J. Norris[1]†

Colloidal quantum dots are robust, efficient, and tunable emitters now used in lighting, displays, and lasers. Consequently, when the spaser—a laser-like source of high-intensity, narrow-band surface plasmons—was first proposed, quantum dots were specified as the ideal plasmonic gain medium for overcoming the significant intrinsic losses of plasmons. Many subsequent spasers, however, have required a single material to simultaneously provide gain and define the plasmonic cavity, a design unable to accommodate quantum dots and other colloidal nanomaterials. In addition, these and other designs have been ill suited for integration with other elements in a larger plasmonic circuit, limiting their use. We develop a more open architecture that decouples the gain medium from the cavity, leading to a versatile class of quantum dot–based spasers that allow controlled generation, extraction, and manipulation of plasmons. We first create aberration-corrected plasmonic cavities with high quality factors at desired locations on an ultrasmooth silver substrate. We then incorporate quantum dots into these cavities via electrohydrodynamic printing or drop-casting. Photoexcitation under ambient conditions generates monochromatic plasmons (0.65-nm linewidth at 630 nm, Q ~ 1000) above threshold. This signal is extracted, directed through an integrated amplifier, and focused at a nearby nanoscale tip, generating intense electromagnetic fields. More generally, our device platform can be straightforwardly deployed at different wavelengths, size scales, and geometries on large-area plasmonic chips for fundamental studies and applications.

INTRODUCTION

Plasmons are surface-bound electromagnetic waves that propagate along metal interfaces (*1*). If their motion is confined in a cavity between two plasmonic reflectors, only standing waves (or modes) at specific wavelengths are permitted. By adding a gain medium that provides energy at these wavelengths, plasmonic losses can be compensated (*2*). Specifically, propagating plasmons can stimulate the emission of additional plasmons, introducing amplification. When the gain exceeds losses for a specific cavity mode, the plasmonic analog of a laser, or spaser, results. An intense narrowband plasmonic signal is produced that can then be extracted for use. For example, by routing this signal toward a sharp tip, monochromatic plasmons can be concentrated in nanoscale volumes for enhancing light-matter interactions.

In the original spaser proposal (*3*, *4*), both the generation and concentration of plasmons occurred within the same nanoscale cavity—a metallic particle coated with colloidal quantum dots. Quantum dots (*5*) were specified for gain because of their high emission quantum yields (often >90%), large transition dipole moments, good photostability, and ability to be packed densely without suffering the self-quenching effects observed in dyes. These properties, in addition to their spectral tunability and solution processability, have made quantum dots attractive emitters for applications in lighting (*6*–*10*), displays (*11*), and lasers (*12*–*15*). However, although the proposed metallic nanoparticle spaser can potentially provide intense local fields, it requires extremely high gain (*16*) and does not produce propagating plasmons. Thus, many efforts have aimed to directly amplifying plasmons propagating within larger devices that exhibit lower losses (*17*–*20*). Plasmon-enhanced lasers have also been investigated (*21*, *22*).

The previous spaser work has followed two general approaches. Top-down nanofabrication has been used to define a semiconductor region that is encased in metal (*20*, *23*), a design that so far has not permitted easy extraction of the cavity plasmons. Alternatively, bottom-up methods have been used to place single-crystalline semiconductor nanowires (*17*, *19*) or nanoflakes (*18*) on a dielectric-coated metal surface. The volume between the metal, the nanostructure, and its end facets define the plasmonic cavity. However, this approach, which exploits the high gain of single-crystalline semiconductors to overcome the modest reflectivity at their facets, has not been amenable to a broader class of useful colloidal nanomaterials. Notably, colloidal-quantum-dot spasers have not been realized despite the long use of these materials in lasers (*12*–*15*). In addition, because the nanowires or nanoflakes are randomly positioned on a surface, they are difficult to integrate with other elements on a chip.

To address these issues, we have applied a hybrid strategy in which we separately engineer the plasmonic cavity and the gain medium. We first optimized the cavity by defining and positioning reflectors for propagating plasmons on a metal surface via lithography. In addition to high reflectivity and placement accuracy, this results in an open and adaptable cavity design that allows quantum dots (or another colloidal nanomaterial) to be easily added for gain. Our strategy also focused on the versatility of the structure while compromising on its dimensions. When extreme confinement of the generated plasmons is desired, our spaser signal can be concentrated outside the cavity through an additional integrated element, as shown below.

RESULTS

Device fabrication and optical characterization

Our cavities consist of two 400- to 600-nm-tall Ag block reflectors protruding from an ultrasmooth Ag surface (Fig. 1A). These blocks provide the in-plane plasmon reflectivity (>90%) (*24*, *25*) necessary

[1]Optical Materials Engineering Laboratory, ETH Zurich, 8092 Zurich, Switzerland.
[2]Laboratory of Thermodynamics in Emerging Technologies, ETH Zurich, 8092 Zurich, Switzerland.
*These authors contributed equally to this work.
†Corresponding author. Email: dnorris@ethz.ch

to obtain high quality factor (Q) cavities. To produce these structures, we first created the inverse of the desired pattern on a [100]-oriented Si wafer with electron beam lithography and reactive ion etching. After thermal evaporation of Ag (*26*) onto the Si template, we peeled off the Ag film with epoxy via template stripping (*27*). By reusing the Si template, many copies of the same chip could be obtained. We then placed CdSe/CdS/ZnS core/shell/shell quantum dots (*25*, *28*, *29*) directly onto the planar Ag surface between the reflectors using electrohydrodynamic NanoDrip printing (Fig. 1B) (*30*, *31*). With the combined capabilities of electron beam lithography and NanoDrip printing, devices can be designed and positioned at will (Fig. 1C).

In conventional laser cavities, stable modes are supported between aberration-corrected concave mirrors (*32*). Analogously, our plasmonic reflectors were designed with a parabolic correction to produce cavities with stable, well-defined plasmonic modes (see sections S1 to S3). We focused on cavities with reflectors 10 μm apart with a radius of curvature at their apex twice their spacing ($R = 2L$ cavity). The spatial profile of the resulting mode, calculated using a simple ray-tracing and reflection algorithm, is highlighted in red in Fig. 2A.

To spectrally characterize the modes of our cavities when empty, we printed ~100 quantum dots at their center. Photoexcitation of the quantum dots launches plasmons into cavity modes (*31*). Some of these plasmons scatter into photons at the outer edge of the block reflector. Thus, by measuring the far-field scattering spectrum, the cavity modes within the quantum dot emission bandwidth can be revealed. Figure 2B compares the measured (red curve) and predicted (gray curve) modes for a 10-μm cavity (see section S4). The slight offset between the two is consistent with a slightly smaller experimental cavity (9.965 μm). The measured linewidths were typically 3 nm (9 meV). For a perfect structure, we predicted linewidths of 2.2 nm (6.8 meV) when we included the finite reflectivity of the blocks and the measured permittivity for our Ag.

Spatially, calculations suggest that these modes have a ~1-μm beam waist (Fig. 2A) and are confined within ~100 nm of the surface when the quantum dot layer is present (see figs. S1 and S2). Thus, to ensure spatial overlap and maximize gain for spasing, we printed quantum dot stripes that were 2 μm wide and at least 100 nm thick (Fig. 2D and fig. S3). We emphasize that the smallest dimension of the device, the thickness of the gain layer, necessitates the use of surface plasmons confined below the diffraction limit of light for adequate overlap. Low-intensity photoexcitation then yielded cavity spectra as in Fig. 2C. Because of losses from the quantum dots, particularly absorption, the modes broaden and only ripples appear on the long-wavelength side. The spectral mode separation also decreases due to the higher refractive index n in the cavity because of the quantum dot layer (Fig. 2C, gray curve).

Characterization of spasing

Under pulsed excitation, the cavity spectra change significantly with increasing power density. At 130 μJ/cm^2 (Fig. 2E), a small feature appears near the middle of the spectrum at a plasmonic mode position. At 250 μJ/cm^2 (Fig. 2F), this feature becomes much sharper and more intense. The insets in Fig. 2 (E and F) show real-space images (false color) of the same cavities. At 250 μJ/cm^2, photon emission from the cavity center greatly decreases, whereas scattering from the reflectors increases. These changes in both the spectral and spatial distribution of scattered plasmons with increasing excitation are consistent with stimulated emission and amplification of plasmons into a single mode defined by the cavity, that is, the onset of spasing.

Quantum dots allow the wavelength of this effect to be easily tuned (Fig. 3A). We fabricated devices with 602-, 625-, and 633-nm-emitting quantum dots. Some devices (see 633 in Fig. 3A) exhibited single-mode operation with typical linewidths of 2 meV, or 0.65 nm, indicating a Q approaching 1000 (Fig. 3B). Other devices (see 602 and 625 in Fig. 3A) showed multiple modes that changed in relative intensity with increasing excitation. Such mode competition, common in lasers (*32*), should also occur in spasers (*33*).

Figure 3C shows the output power spectrally integrated over the peak of the single-mode 633 device as a function of excitation power (red). A noticeable inflection occurs at ~180 μJ/cm^2, with a concurrent decrease in spectral linewidth (blue) that corresponds to the spasing threshold. (Other devices had values down to 100 μJ/cm^2.) This is somewhat surprising given that the best quantum dot lasers, which

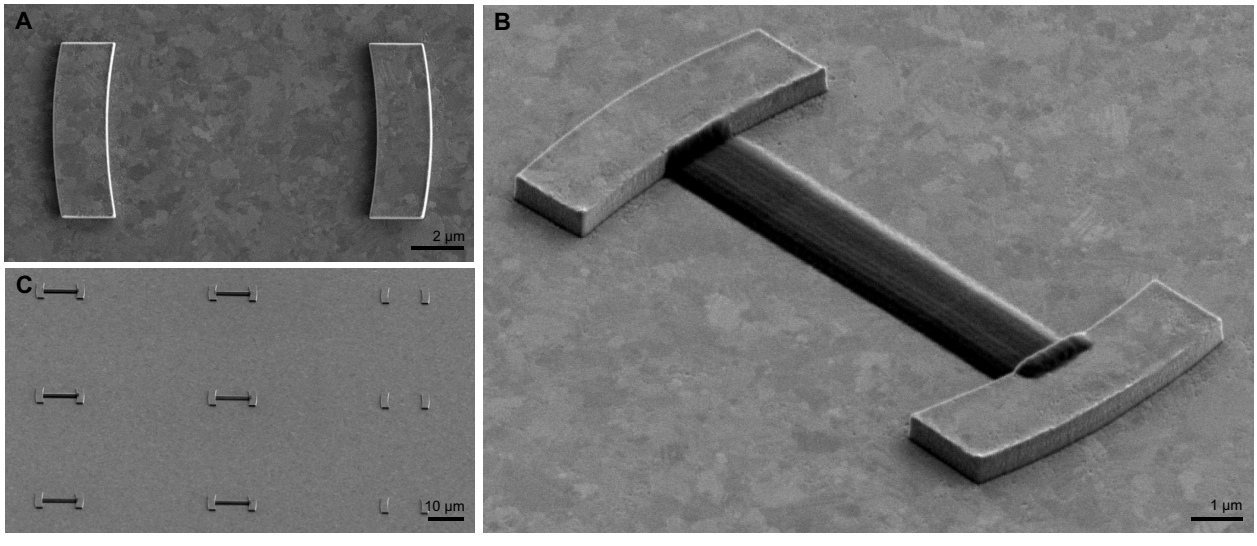

Fig. 1. Structure of colloidal quantum dot spaser. (**A**) Top-view electron micrograph of a plasmonic cavity: Two ~600-nm-tall Ag block reflectors positioned 10 μm apart on an ultrasmooth Ag surface. The blocks can be designed and placed at will. Plasmons propagate between the reflectors to create a cavity. (**B**) Tilted view of a functional device. NanoDrip printing is used to deposit a stripe (~100 nm thick and ~2 μm wide) of colloidal quantum dots between the reflectors. (**C**) Tilted view of a square array of nine plasmonic cavities (50 μm apart). The three cavities in the right column are empty. The rest contain a quantum dot stripe, as in (B).

should have lower losses, exhibit comparable values (*14*). Although this certainly attests to the quality of our devices, other factors must be involved. Thresholds can be reduced in spasers due to the Purcell enhancement of the quantum dot emission rate and high coupling of this emission to the cavity mode. An estimate of the threshold based on experimental parameters (*34*) gives good agreement with measured values (see sections S6 to S9 and figs. S4 and S5 for further discussion).

Green-emitting quantum dots did not exhibit spasing, presumably due to increased plasmonic losses at shorter wavelengths. However, at very high excitation intensities (~1000 μJ/cm^2), new spectral features appeared for our red-emitting quantum dots (Fig. 3D). Under these conditions, higher-energy multiexcitons (emitting around 590 nm) are generated in the quantum dots, providing sufficient gain (*35*) for spasing at shorter wavelengths (578 nm). Moreover, a progression of spasing modes was observed with spacings in agreement with calculations assuming n = 1.60 for the quantum dot film (Fig. 3D, dotted curve). Although this refractive index is smaller than that measured via ellipsometry (1.75), these high exciton populations can significantly decrease n (*36*). A lower n also agrees with observed blue shifts in the spasing modes with increased excitation.

Extracting the spaser signal from the cavity for on-chip use

Having demonstrated spasing, we now extract this signal for potential on-chip use. Our device architecture allows for straightforward integration of a plasmonic waveguide simply by extending the reflector. Moreover, as the plasmons propagate out of the cavity along the waveguide, they can be focused to the nanoscale by tapering (*37*). Figure 4A shows a cavity in which one reflector has been extended ~35 μm and narrowed to a tip. Figure 4B presents the same device operating above threshold. The contrast has been enhanced (10^4) in the right-hand portion of the image to resolve plasmons that are guided and focused. The cavity spectrum (Fig. 4C) matches that of plasmons scattered at the tip (Fig. 4D). Thus, the spaser signal is extracted, guided, and focused, but with diminished intensity due to modest outcoupling and propagation losses.

The tip signal can be further enhanced if the spaser is combined with a plasmonic amplifier. Although this could be achieved by printing

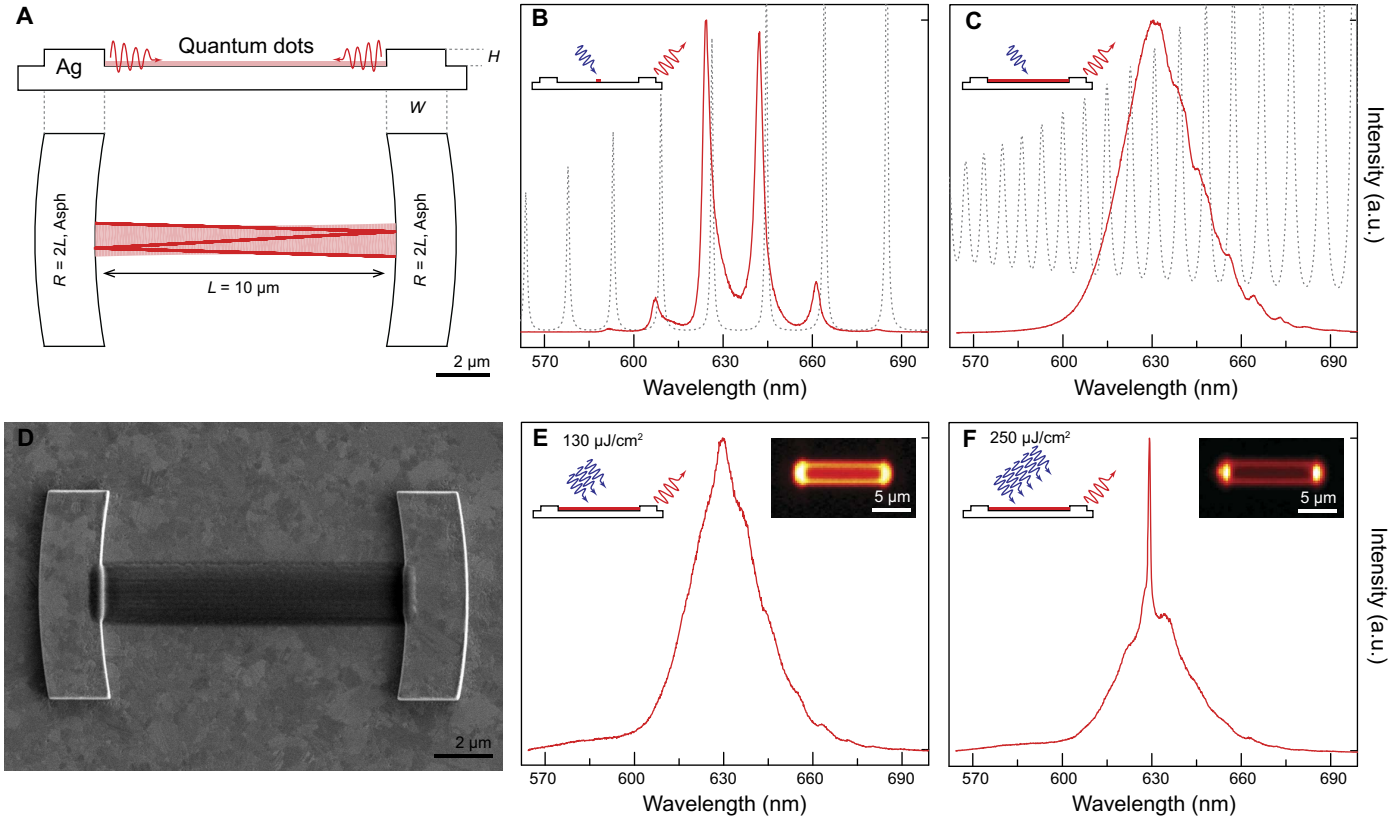

Fig. 2. Design and characterization of plasmonic cavities containing quantum dots. (**A**) The plasmonic reflectors are designed with a radius of curvature twice the cavity length (R = 2L cavity) and include a parabolic correction. Plasmons emitted into the cavity are spatially confined in a stable cavity mode, depicted in red. (**B**) When ~100 quantum dots are placed in the cavity and weakly photoexcited, they emit into plasmonic cavity modes. The experimental cavity spectrum, measured by detecting plasmons scattered into the far field at the outer edge of one of the reflectors, is shown in red. The calculated spectra of the stable plasmonic cavity modes are in gray (see sections S4 and S5). The slight offset is due to a slightly smaller experimental cavity length (9.965 μm). (**C**) When a cavity filled with quantum dots as in (D) is weakly photoexcited, modes appear as ripples in the cavity spectrum [collected as in (B)] only at longer wavelengths due to losses from the quantum dot film. Calculated modes (neglecting quantum dot absorption) are in gray. a.u., arbitrary units. (**D**) Top-view electron micrograph of the cavity for comparison with (A). The quantum dot stripe is printed to maximize spatial overlap with the cavity mode. (**E**) Under pulsed excitation (130 μJ/cm^2), a small feature rises on top of the cavity spectrum at the position of a calculated plasmonic mode. Right inset: Real-space image (false color) of the emission from the quantum dot stripe. The two bright spots are due to scattering off the reflectors. (**F**) At higher excitation (250 μJ/cm^2), the small peak in (E) narrows and increases in intensity. Right inset: Real-space image as in (E). The device exhibits decreased emission within the stripe and increased signal at the reflectors. The changes in the spectra and images in (E) and (F) are indicative of the onset of spasing. Cartoons in (B) and (D) to (F) depict the optical excitation and collection processes.

quantum dots on the waveguide, we took advantage of the solution processability of colloidal nanomaterials and developed a simple drop-casting method that conformally coats our entire chip with a ~150-nm-thick film of quantum dots. Figure 4 (E and F) shows this approach applied to an extended reflector cavity (14° taper). Below threshold (Fig. 4E), broadband emission is observed that is fairly uniform with some guiding and focusing of plasmons at the tip. Above threshold (Fig. 4F), the spatial intensity distribution completely changes. The output of the spaser is amplified as it travels toward the tip, leading to highly concentrated plasmons (*37*). The emission from the tip in Fig. 4H with amplification is more than 10^3 times stronger than that in Fig. 4D without amplification. When comparing the spectrum from the cavity (Fig. 4G) with that from the tip (Fig. 4H), we observe the same modes. However, at the tip, spontaneous emission is diminished and a single spaser mode is selectively amplified. At higher excitation intensities, unwanted amplified spontaneous emission can occur from the amplifier alone (see fig. S6). However, this leads to many finely spaced features, unrelated to the cavity modes, in the tip spectrum.

DISCUSSION

Our devices represent the intersection of several key advances in nanofabrication. High-quality plasmonic resonators arose from improvements in our ability (i) to deposit Ag films with superior dielectric properties and (ii) to sculpt high aspect ratio structures of arbitrary geometries from these films. Analogously, the progression of colloidal quantum dot synthesis has led to increasingly compact, bright, and photostable emitters for high gain. Finally, these advanced

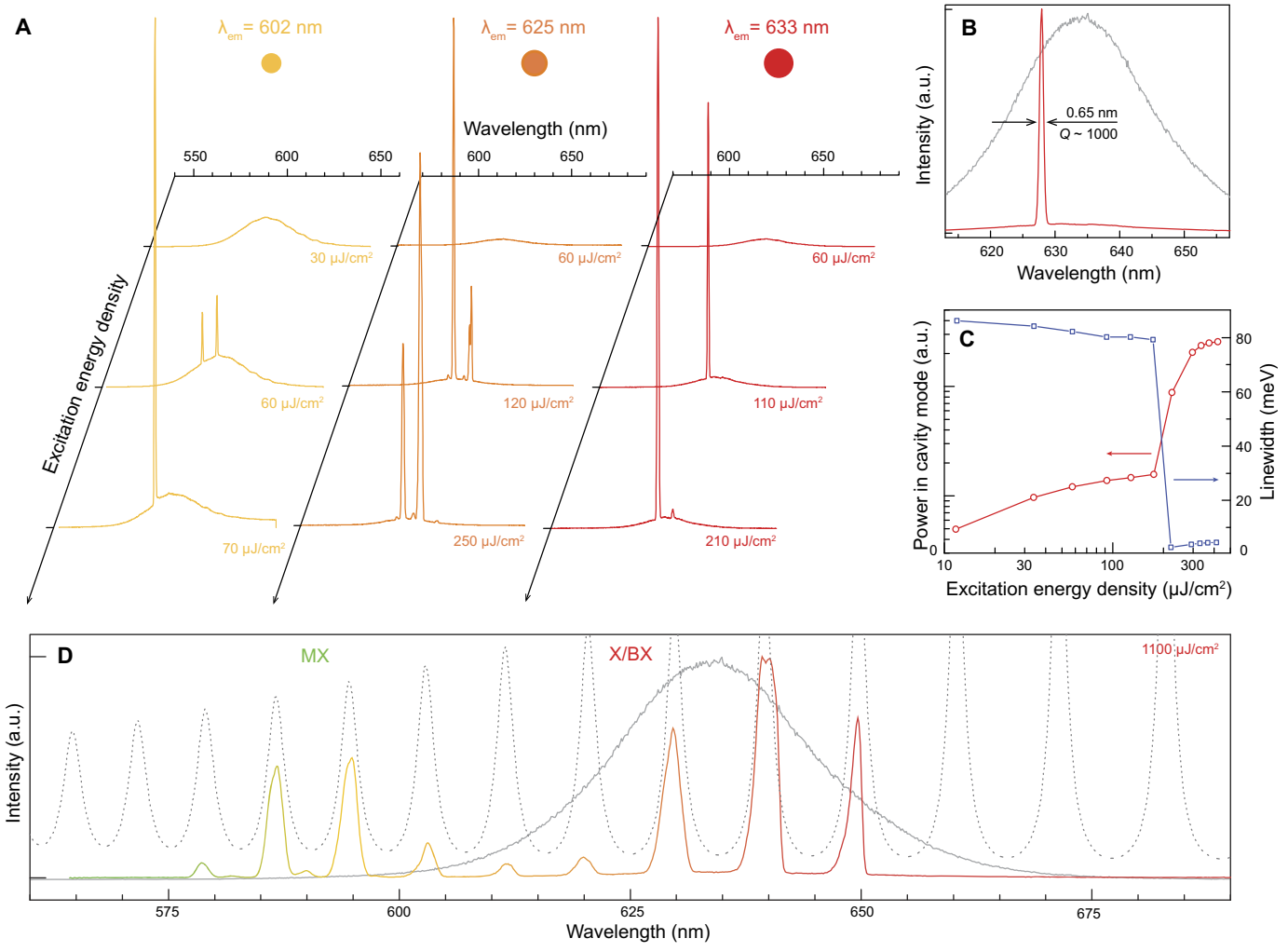

Fig. 3. Analysis of quantum dot spasers. (**A**) Quantum dot samples with emission centered at 602, 625, and 633 nm were used to fabricate spasers. Cavity spectra for each are plotted for three excitation intensities, one below and two above threshold. (**B**) The 633 device from (A) exhibited a single spasing mode above threshold (red curve). Typical linewidths were 2 meV (0.65 nm, Q ~ 1000). The broad photoluminescence spectrum from quantum dots on flat Ag (outside the cavity) is shown for comparison (gray curve). (**C**) The input-output power plot of the 633 device (red points) reveals an inflection at ~180 μJ/cm^2. Spasing thresholds as low as ~100 μJ/cm^2 were observed. The spectral full-width at half-maximum (blue points) decreases dramatically at the same inflection point, consistent with the onset of spasing. (**D**) When the 633 device is excited at very high intensities (~1000 μJ/cm^2), a progression of spasing modes is observed. These occur within the gain envelopes of the exciton/biexciton (X/BX) centered at ~640 nm and the multiexcitons (MX) centered at ~590 nm. The ~160-meV spacing between the envelopes is consistent with previous measurements (*35*). The broad quantum dot spectrum (solid gray curve) from (B) and the expected plasmonic modes for a film with n = 1.60 (dashed gray curve) are shown for comparison.

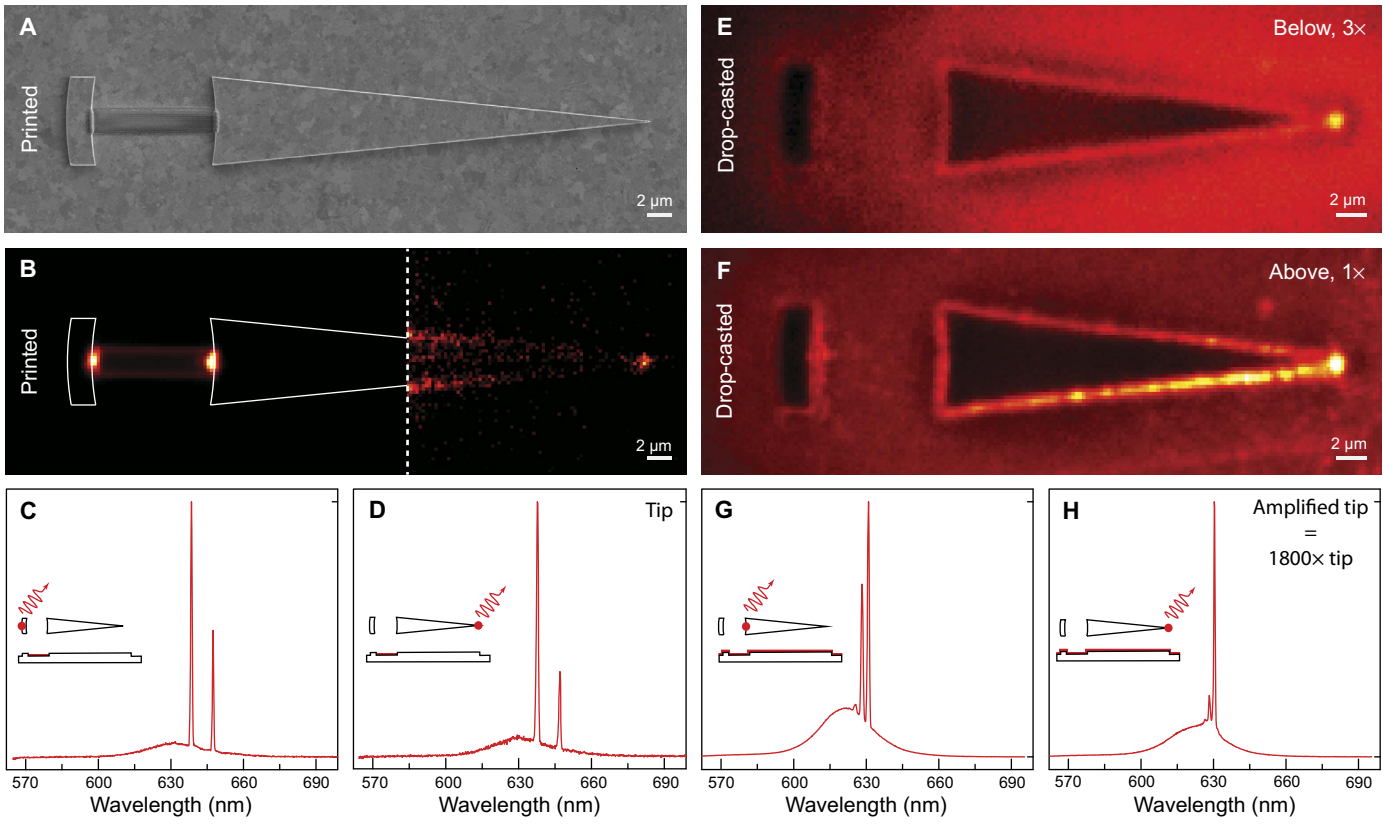

Fig. 4. Extraction, amplification, and focusing of plasmons generated by quantum dot spasers. (**A**) Top-view electron micrograph of a spaser with a printed quantum dot stripe and an elongated reflector (11.5° taper) to guide and nanofocus the spaser signal. (**B**) Real-space image (false color) of the device in (A) above threshold. The contrast of the image to the right of the vertical dashed line is enhanced (10^4) to show the plasmons focused at the tip. (**C** and **D**) Spectra measured by collecting plasmons scattered at the outer reflector edge (C) and the tip (D) confirm that the spasing signal is guided and focused. (**E** and **F**) Real-space images (false color) of a cavity with an elongated reflector (14° taper) coated with a ~150-nm-thick drop-casted quantum dot film, excited below and above threshold, respectively. The intensity of (E), which is multiplied by 3, is fairly uniform across the device with some broadband focusing at the tip. In (F), plasmons generated by the cavity are amplified and focused at the tip. (**G** and **H**) Spectra measured by collecting plasmons scattered at the inner reflector edge (G) and the tip (H) confirm that a single spasing mode is selectively guided, amplified, and focused. The signal in (H) (with amplification) is 1800 times greater than that in (D) (without amplification).

materials were unified to create a device framework via developments in both micro- and macroscale deposition of colloidal nanoparticles.

Here, we have focused on demonstrating the versatility and potential of our spaser platform by characterizing a small subset of its vast design space. This space can be readily explored and characterized given the ease of fabrication—a single template-stripped substrate followed by drop-casting creates a chip containing many arrays of devices. Our spasers operated under air at room temperature with near-unity yield (108 of 112, or 96% of our measured drop-casted devices showed spasing). In addition, the size of these devices can be modified. Preliminary explorations of different cavity designs have shown that quantum dot spasers with cavity lengths down to at least 2 μm can be obtained.

The open-cavity nature of our platform permits access to the spasing modes within the cavity. This allows for direct measurements of these modes, for example, by using near-field techniques, for studying plasmonic cavity physics. One application where this open-cavity feature could be particularly useful is in plasmonic sensing. The figure of merit for plasmonic sensing is inversely proportional to the spectral linewidth of the surface plasmon signal. Because our spasers generate plasmons of very narrow linewidth (Q ~ 1000), they are good candidates for refractive index sensing. Moreover, due to several decades of research, the surface functionalization of colloidal quantum dots is quite advanced. This can be combined with the open-cavity design to enable targeting of specific analytes. Consequently, the quantum dot spaser can conceivably provide a route to high-sensitivity and high-specificity sensors.

Although we have presented individual functional units consisting of a spaser, amplifier, and waveguide, many such units can be linked to build an integrated circuit. Going beyond block reflectors, elements such as plasmonic antennas and gratings could be implemented within the current scheme. Quantum dots (or other gain media such as organic-inorganic perovskites and rare earth–doped oxides) can then be deposited where needed for spasing and signal amplification. The flexibility and broad applicability of this framework may enable the practical implementation of spasers for future integrated plasmonic applications.

MATERIALS AND METHODS

Plasmonic cavity fabrication

Si(001) wafers (50.8 mm diameter) with a native oxide layer were used as the template. After a prebake step (180°C for 10 min), ~280 nm of an electron beam resist (Allresist, CSAR 62 AR-P 6200) was spin-cast onto each wafer (2000 rpm for 60 s). This was followed by a postbake step (150°C for 5 min). The resist was exposed using an electron beam lithography system (Vistec, EBPG5200; acceleration voltage, 100 kV;

aperture size, 300 μm; and base dose, 290 μC/cm^2). After exposure, the resist was developed (Allresist, AR 600-546), and the Si was etched using an inductively coupled plasma deep reactive ion etch (Oxford, Plasmalab System 100, HBr, 40 sccm, 80 W radio frequency). Afterward, the remaining resist was removed using oxygen plasma (100 W, 5 min) and exposure to *N*-methyl-2-pyrrolidone (>60 min at 130°C; Sigma-Aldrich). After a rinse with isopropanol, the Si templates were loaded into a thermal evaporator (Kurt J. Lesker, NANO 36) containing a homebuilt rotating sample holder tilted 30° from horizontal. About 1 μm of Ag (Kurt J. Lesker, 99.99%) was deposited at 50 Å/s under a chamber gas pressure of <10^{-7} torr while the sample rotated at ~60 rpm. After evaporation, the plasmonic cavities were manually template-stripped from the Si using a glass microscope slide bonded to the surface with an ultraviolet light-curable epoxy (Epoxy Technology, OG142-95) (*25*, *27*). The direction of template stripping was chosen to minimize structural defects at the reflector walls.

Quantum dot synthesis

Core/shell/shell CdSe/CdS/ZnS colloidal quantum dots were synthesized according to previously published recipes (*25*). Their color was tuned by using smaller CdSe cores while adjusting the shells accordingly.

Localized quantum dot printing

Quantum dots were transferred from hexane to tetradecane through selective evaporation. The concentration was adjusted to an absorbance of 0.5 at the lowest energy exciton absorption feature for a 1-mm path length. These inks were further diluted 1:3, 1:2, and 1:5 in tetradecane for the 602-, 625-, and 633-nm-emitting quantum dots, respectively. A description of the electrohydrodynamic NanoDrip printing setup can be found elsewhere (*30*). In addition, a 50× objective [Edmund Optics, Plan Apo ULWD; numerical aperture (NA), 0.42; working distance, 20.5 mm] was mounted at an angle of 45° for live inspection. Printing nozzles were fabricated by pulling glass capillaries (TW100-4, World Precision Instruments) using a Sutter Instruments P-97 pipette puller. These were then coated (electron beam evaporation, Plassys, MEB550S) with a 10-nm titanium adhesion layer and a 100-nm layer of gold. The outer diameter of the nozzles was in the range of 1800 to 2000 nm. A dc electric potential of ~250 V was applied between the nozzle (+) and the template-stripped silver substrate (ground). The separation between the nozzle tip and the substrate was 5 μm. The 10-μm-long, 2-μm-wide, and ~100- to 400-nm-thick quantum dot stripes (for example, see Fig. 2C) were deposited by moving the substrate with a velocity of 6 μm/s in a serpentine-like and layer-by-layer fashion with a line pitch of 160 nm. Seven to 16 layers were added to obtain the desired thicknesses. Atomic force microscope (AFM) topographical images (see fig. S3) were measured in tapping mode with a Bruker Dimension FastScan AFM with a TESPA-V2 tip (8-nm tip radius).

Optical characterization: Optical pumping, imaging, and spectroscopy

For weak optical excitation (Fig. 2, B and D), a white-light light-emitting diode (Lumencor, SOLA SE II Light Engine) was used in conjunction with a dichroic beam splitter (488-nm long pass, AHF analysentechnik). The remaining images and spectra were obtained using a pulsed source. Pulses (450 nm; pulse duration, ~340 fs; repetition rate, 1 KHz) were generated by a collinear optical parametric amplifier (Spectra-Physics, Spirit-OPA) pumped by a 1040-nm pump laser (Spectra-Physics, Spirit-1040-8). After spectral filtering, the beam was directed through a gradient neutral density filter wheel to adjust the pulse power (Thorlabs, NDC-50C-2M-B). After beam expansion and collimation, a small portion of the beam was directed to a photodiode to monitor the pump power (Thorlabs, DET110). The remainder of the beam was passed through a defocusing lens (focal length of 150 mm) into an inverted microscope (Nikon, Eclipse Ti-U). The beam was then directed upward to the sample using a dichroic beam splitter (488-nm long pass, AHF analysentechnik) through a 50× air objective (Nikon, TU Plan Fluor, 0.8 NA).

The defocusing lens was adjusted to provide a spot size of 60 to 70 μm. The spot size was determined from an image of the photoluminescence from a flat portion of a film of quantum dots. A cross-section of the spot was then fitted with the sum of two Gaussian functions, and the full-width at half-maximum was determined numerically. The excitation power density at the sample was monitored by correlating the power meter reading above the objective at the sample plane (Thorlabs, S170C with PM100D) with the electrical current reading from the photodiode.

Emission from the sample was collected by the same objective and directed through the dichroic beam splitter, emission filter (500-nm long pass, AHF analysentechnik) and relay lenses (focal length of 200 mm) into an imaging spectrometer (Andor, Shamrock 303i). The emission was dispersed with a grating of 300 lines/mm (500-nm blaze) and imaged with an air-cooled electron-multiplying charged-coupled device camera (Andor, iXon 888 Ultra). Real-space images were obtained using the zero-order mode of the same grating.

Large-area quantum dot drop-casting

Template-stripped plasmonic cavities were cooled to 5°C on a copper block partially submerged in a solvent bath containing benzene and dry ice inside a homebuilt glovebox purged with dry N_2 gas. Twenty microliters of a dispersion of quantum dots with an absorbance of 0.92 at the lowest energy exciton absorption feature for a 1-mm path length was used for drop-casting. Samples were allowed to dry on top of the block before warming up to room temperature within the glovebox.

SUPPLEMENTARY MATERIALS

Supplementary material for this article is available at http://advances.sciencemag.org/cgi/content/full/3/9/e1700688/DC1

section S1. Computation of mode stability
section S2. Beam waist calculation and ray tracing
section S3. Cavity design
section S4. Plasmonic Fabry-Perot calculation for cavities
section S5. Calculation of propagating modes in silver/quantum dot/air stack
section S6. Optical characterization: Lifetime measurements
section S7. Spasing thresholds
section S8. Modal gain, plasmonic loss, and quantum dot material gain
section S9. Estimation of spasing threshold
table S1. Parameters for threshold calculation.
fig. S1. Calculated electric field profiles.
fig. S2. Calculated effective indices for plasmonic and photonic modes.
fig. S3. AFM topographic image of a printed quantum dot stripe.
fig. S4. Lifetime measurements.
fig. S5. Measuring amplifier gain.
fig. S6. Amplified spontaneous emission at high excitation intensity.
References (*38*–*40*)

REFERENCES AND NOTES

1. S. A. Maier, *Plasmonics: Fundamentals and Applications* (Springer Science, 2007).
2. P. Berini, I. De Leon, Surface plasmon–polariton amplifiers and lasers. *Nat. Photonics* **6**, 16–24 (2012).
3. M. I. Stockman, Spasers explained. *Nat. Photonics* **2**, 327–329 (2008).
4. D. J. Bergman, M. I. Stockman, Surface plasmon amplification by stimulated emission of radiation: Quantum generation of coherent surface plasmons in nanosystems. *Phys. Rev. Lett.* **90**, 027402 (2003).

5. V. I. Klimov, *Nanocrystal Quantum Dots* (CRC Press, ed. 2, 2010).
6. V. L. Colvin, M. C. Schlamp, A. P. Alivisatos, Light-emitting diodes made from cadmium selenide nanocrystals and a semiconducting polymer. *Nature* **370**, 354–357 (1994).
7. P. O. Anikeeva, J. E. Halpert, M. G. Bawendi, V. Bulović, Quantum dot light-emitting devices with electroluminescence tunable over the entire visible spectrum. *Nano Lett.* **9**, 2532–2536 (2009).
8. L. Qian, Y. Zheng, J. Xue, P. H. Holloway, Stable and efficient quantum-dot light-emitting diodes based on solution-processed multilayer structures. *Nat. Photonics* **5**, 543–548 (2011).
9. Y. Shirasaki, G. J. Supran, M. G. Bawendi, V. Bulović, Emergence of colloidal quantum-dot light-emitting technologies. *Nat. Photonics* **7**, 13–23 (2013).
10. X. Dai, Z. Zhang, Y. Jin, Y. Niu, H. Cao, X. Liang, L. Chen, J. Wang, X. Peng, Solution-processed, high-performance light-emitting diodes based on quantum dots. *Nature* **515**, 96–99 (2014).
11. T.-H. Kim, K.-S. Cho, E. K. Lee, S. J. Lee, J. Chae, J. W. Kim, D. H. Kim, J.-Y. Kwon, G. Amaratunga, S. Y. Lee, B. L. Choi, Y. Kuk, J. M. Kim, K. Kim, Full-colour quantum dot displays fabricated by transfer printing. *Nat. Photonics* **5**, 176–182 (2011).
12. V. I. Klimov, A. A. Mikhailovsky, S. Xu, A. Malko, J. A. Hollingsworth, C. A. Leatherdale, H.-J. Eisler, M. G. Bawendi, Optical gain and stimulated emission in nanocrystal quantum dots. *Science* **290**, 314–317 (2000).
13. V. I. Klimov, S. A. Ivanov, J. Nanda, M. Achermann, I. Bezel, J. A. McGuire, A. Piryatinski, Single-exciton optical gain in semiconductor nanocrystals. *Nature* **447**, 441–446 (2007).
14. C. Dang, J. Lee, C. Breen, J. S. Steckel, S. Coe-Sullivan, A. Nurmikko, Red, green and blue lasing enabled by single-exciton gain in colloidal quantum dot films. *Nat. Nanotechnol.* **7**, 335–339 (2012).
15. A. Nurmikko, What future for quantum dot-based light emitters? *Nat. Nanotechnol.* **10**, 1001–1004 (2015).
16. J. B. Khurgin, How to deal with the loss in plasmonics and metamaterials. *Nat. Nanotechnol.* **10**, 2–6 (2015).
17. R. F. Oulton, V. J. Sorger, T. Zentgraf, R.-M. Ma, C. Gladden, L. Dai, G. Bartal, X. Zhang, Plasmon lasers at deep subwavelength scale. *Nature* **461**, 629–632 (2009).
18. R.-M. Ma, R. F. Oulton, V. J. Sorger, G. Bartal, X. Zhang, Room-temperature sub-diffraction-limited plasmon laser by total internal reflection. *Nat. Mater.* **10**, 110–113 (2011).
19. Y. J. Lu, J. Kim, H.-Y. Chen, C. Wu, N. Dabidian, C. E. Sanders, C.-Y. Wang, M.-Y. Lu, B.-H. Li, X. Qiu, W.-H. Chang, L.-J. Chen, G. Shvets, C.-K. Shih, S. Gwo, Plasmonic nanolaser using epitaxially grown silver film. *Science* **337**, 450–453 (2012).
20. M. T. Hill, M. Marell, E. S. P. Leong, B. Smalbrugge, Y. Zhu, M. Sun, P. J. van Veldhoven, E. J. Geluk, F. Karouta, Y.-S. Oei, R. Nötzel, C.-Z. Ning, M. K. Smit, Lasing in metal-insulator-metal sub-wavelength plasmonic waveguides. *Opt. Express* **17**, 11107–11112 (2009).
21. W. Zhou, M. Dridi, J. Y. Suh, C. H. Kim, D. T. Co, M. R. Wasielewski, G. C. Schatz, T. W. Odom, Lasing action in strongly coupled plasmonic nanocavity arrays. *Nat. Nanotechnol.* **8**, 506–511 (2013).
22. T. K. Hakala, H. T. Rekola, A. I. Väkeväinen, J.-P. Martikainen, M. Nečada, A. J. Moilanen, P. Törmä, Lasing in dark and bright modes of a finite-sized plasmonic lattice. *Nat. Commun.* **8**, 13687 (2017).
23. M. Khajavikhan, A. Simic, M. Katz, J. H. Lee, B. Slutsky, A. Mizrahi, V. Lomakin, Y. Fainman, Thresholdless nanoscale coaxial lasers. *Nature* **482**, 204–207 (2012).
24. G. Brucoli, L. Martin-Moreno, Effect of defect depth on surface plasmon scattering by subwavelength surface defects. *Phys. Rev. B* **83**, 075433 (2011).
25. S. J. P. Kress, F. V. Antolinez, P. Richner, S. V. Jayanti, D. K. Kim, F. Prins, A. Riedinger, M. P. C. Fischer, S. Meyer, K. M. McPeak, D. Poulikakos, D. J. Norris, Wedge waveguides and resonators for quantum plasmonics. *Nano Lett.* **15**, 6267–6275 (2015).
26. K. M. McPeak, S. V. Jayanti, S. J. P. Kress, S. Meyer, S. Iotti, A. Rossinelli, D. J. Norris, Plasmonic films can easily be better: Rules and recipes. *ACS Photonics* **2**, 326–333 (2015).
27. P. Nagpal, N. C. Lindquist, S.-H. Oh, D. J. Norris, Ultrasmooth patterned metals for plasmonics and metamaterials. *Science* **325**, 594–597 (2009).
28. O. Chen, J. Zhao, V. P. Chauhan, J. Cui, C. Wong, D. K. Harris, H. Wei, H.-S. Han, D. Fukumura, R. K. Jain, M. G. Bawendi, Compact high-quality CdSe–CdS core–shell nanocrystals with narrow emission linewidths and suppressed blinking. *Nat. Mater.* **12**, 445–451 (2013).
29. K. Boldt, N. Kirkwood, G. A. Beane, P. Mulvaney, Synthesis of highly luminescent and photo-stable, graded shell CdSe/$Cd_xZn_{1-x}S$ nanoparticles by in situ alloying. *Chem. Mater.* **25**, 4731–4738 (2013).
30. P. Galliker, J. Schneider, H. Eghlidi, S. Kress, V. Sandoghdar, D. Poulikakos, Direct printing of nanostructures by electrostatic autofocussing of ink nanodroplets. *Nat. Commun.* **3**, 890 (2012).
31. S. J. P. Kress, P. Richner, S. V. Jayanti, P. Galliker, D. K. Kim, D. Poulikakos, D. J. Norris, Near-field light design with colloidal quantum dots for photonics and plasmonics. *Nano Lett.* **14**, 5827–5833 (2014).
32. A. E. Siegman, *Lasers* (University Science Books, 1986).
33. M. C. Gather, A rocky road to plasmonic lasers. *Nat. Photonics* **6**, 708 (2012).
34. S.-L. Chua, B. Zhen, J. Lee, J. Bravo-Abad, O. Shapira, M. Soljačić, Modeling of threshold and dynamics behavior of organic nanostructured lasers. *J. Mater. Chem. C* **2**, 1463–1473 (2014).
35. B. Fisher, J.-M. Caruge, Y.-T. Chan, J. Halpert, M. G. Bawendi, Multiexciton fluorescence from semiconductor nanocrystals. *Chem. Phys.* **318**, 71–81 (2005).
36. F. Henneberger, Optical bistability at the absorption edge of semiconductors. *Phys. Status Solidi B* **137**, 371–432 (1986).
37. E. Verhagen, A. Polman, L. Kuipers, Nanofocusing in laterally tapered plasmonic waveguides. *Opt. Express* **16**, 45–57 (2008).
38. V. J. Sorger, R. F. Oulton, J. Yao, G. Bartal, X. Zhang, Plasmonic Fabry-Pérot nanocavity. *Nano Lett.* **9**, 3489–3493 (2009).
39. E. Verhagen, thesis, Utrecht University (2009).
40. M. M. Adachi, F. Fan, D. P. Sellan, S. Hoogland, O. Voznyy, A. J. Houtepen, K. D. Parrish, P. Kanjanaboos, J. A. Malen, E. H. Sargent, Microsecond-sustained lasing from colloidal quantum dot solids. *Nat. Commun.* **6**, 8694 (2015).

Acknowledgments: We thank E. De Leo, S. Meyer, Y. Fedoryshyn, and U. Drechsler for experimental assistance. **Funding:** We acknowledge funding from the European Research Council (ERC) under the European Union's Seventh Framework Program (FP/2007-2013)/ERC grant agreement no. 339905 (QuaDoPS Advanced Grant) and from the Swiss National Science Foundation under grant no. 146180. J.C. acknowledges funding from the ETH Zurich Postdoctoral Fellowship Program and the Marie Curie Actions for People COFUND Program. **Author contributions:** S.J.P.K., J.C., and D.J.N. conceived the ideas and planned the experiments. S.J.P.K. designed and fabricated the resonators with assistance from J.C. and K.M.M. D.K.K. synthesized the quantum dots. P. Rohner performed NanoDrip printing with assistance from P. Richner and supervision from D.P. K.-A.Z. developed the drop-casting method. J.C. performed optical measurements with assistance from S.J.P.K. and S.V.J. S.J.P.K., J.C., P. Rohner, and F.V.A. analyzed the data with guidance from D.J.N. S.J.P.K., J.C., and D.J.N. wrote the manuscript with input from all authors. **Competing interests:** D.P. is involved with a start-up company that is attempting to commercialize NanoDrip printing. D.J.N., S.J.P.K., J.C., P. Rohner, F.V.A., K.-A.Z., and S.V.J. are authors on a pending International Patent Application through the European Patent Office (application no. PCT/EP 2017/064041, filed 8 June 2017). The authors declare no other competing interests. **Data and materials availability:** All data needed to evaluate the conclusions in the paper are present in the paper and/or the Supplementary Materials. Additional data related to this paper may be requested from the authors.

Submitted 8 March 2017
Accepted 30 August 2017
Published 22 September 2017
10.1126/sciadv.1700688

Citation: S. J. P. Kress, J. Cui, P. Rohner, D. K. Kim, F. V. Antolinez, K.-A. Zaininger, S. V. Jayanti, P. Richner, K. M. McPeak, D. Poulikakos, D. J. Norris, A customizable class of colloidal-quantum-dot spasers and plasmonic amplifiers. *Sci. Adv.* **3**, e1700688 (2017).